A New 3,5-Bisporphyrinylpyridine Derivative as a Fluorescent Ratiometric Probe for Zinc Ions

ARTICLE *in* CHEMISTRY - A EUROPEAN JOURNAL · APRIL 2014

Impact Factor: 5.73 · DOI: 10.1002/chem.201402270 · Source: PubMed

9 AUTHORS, INCLUDING:

Nuno M. M. Moura
University of Aveiro
18 PUBLICATIONS **110** CITATIONS
SEE PROFILE

Cristina Nuñez
New University of Lisbon
55 PUBLICATIONS **415** CITATIONS
SEE PROFILE

Maria Faustino
University of Aveiro
152 PUBLICATIONS **1,642** CITATIONS
SEE PROFILE

Carlos Lodeiro
University NOVA of Lisbon
239 PUBLICATIONS **3,003** CITATIONS
SEE PROFILE

ChemPubSoc Europe

DOI: 10.1002/chem.201402270

CHEMISTRY
A European Journal
Full Paper

Fluorescent Probes

A New 3,5-Bisporphyrinylpyridine Derivative as a Fluorescent Ratiometric Probe for Zinc Ions

Nuno M. M. Moura,[a, b, c] Cristina Núñez,[b, c, d] Sérgio M. Santos,[e] M. Amparo F. Faustino,[a] José A. S. Cavaleiro,[a] Filipe A. Almeida Paz,[e] M. Graça P. M. S. Neves,*[a] José Luis Capelo,[b, c] and Carlos Lodeiro*[b, c]

Abstract: A new 3,5-disubstituted pyridine with two porphyrin moieties was prepared through an efficient synthetic approach involving 2-formyl-5,10,15,20-tetraphenylporphyrin (**1**), piperidine, and catalytic amounts of $[La(OTf)_3]$. 3,5-Bis(5,10,15,20-tetraphenylporphyrin-2-ylmethyl)pyridine (**2**) was fully characterized and its sensing ability towards Zn^{2+}, Cu^{2+}, Hg^{2+}, Cd^{2+}, and Ag^{+} was evaluated in solution by absorption and fluorescence spectroscopy and in gas phase by using matrix-assisted laser desorption/ionization (MALDI)-TOF mass spectrometry. Strong changes in the ground and excited state were detected in the case of the soft metal ions Zn^{2+}, Cd^{2+}, Hg^{2+}, and Cu^{2+}. A three-metal-per-ligand molar ratio was obtained in all cases and a significant ratiometric behavior was observed in the presence of Zn^{2+} with the appearance of a new band at 608 nm, which can be assigned to a metal-to-ligand charge transfer. The system was able to quantify 79 ppb of Zn^{2+} and the theoretical calculations are in accordance with the stoichiometry observed in solution. The gas-phase sensorial ability of compound **2** towards all metal ions was confirmed by using MALDI-TOF MS and in solid state by using polymeric films of polymethylmethacrylate (PMMA) doped with ligand **2**. The results showed that compound **2** can be analytically used to develop new colorimetric molecular devices that are able to discriminate between Hg^{2+} and Zn^{2+} in solid phase. The crystal structure of Zn^{II} complex of 3,5-bisporphyrinylpyridine was unequivocally elucidated by using single-crystal X-ray diffraction studies.

Introduction

The growing interest in tetrapyrrolic macrocycles, namely on the development of new synthetic strategies to obtain new functional derivatives, is related with their physicochemical features that strongly encourage their application in several fields; indeed, porphyrins are used as catalysts, advanced biomimetic models for photosynthesis, new electronic materials, sensors, and drugs.[1] In particular, porphyrins are considered attractive candidates to be used as fluorescent and colorimetric chemosensors due to their remarkable photophysical properties, such as large Stokes shifts and relatively long excitation (>400 nm) and emission (>600 nm) wavelengths.[2,3] The high interest on the development of probes that are able to detect metal ions by fluorescence or colorimetric changes can be justified by the simplicity, quickness and the low detection limit associated with optical techniques; moreover these inexpensive methods are non-destructive and can be used in bio-imaging.[4–7]

The detection of the soft metal ions such as zinc(II) and copper(II) are of particular interest due to their significant functions on biological and environmental fields.[8–11] Other important metal ions that merit to be studied are mercury(II) and cadmium(II), due to their high toxicity for living organisms,[12] being the selective detection of these metal ions of significant importance for environmental and health-related issues.[13–16]

Most of the work using porphyrins as chemosensors in the detection of metal ions are based on macrocyles functionalized with adequate binding units in *meso* positions,[17] and as far as we know much less attention is being given to porphyrins that are β-functionalized.[18]

Concerning our studies on structural modification of *meso*-tetraarylporphyrins at their β-pyrrolic positions, namely through a formyl group,[19] we report here an efficient and facile access to a new 3,5-di-substituted pyridine bearing two

[a] Dr. N. M. M. Moura, Prof. M. A. F. Faustino, Prof. J. A. S. Cavaleiro, Prof. M. G. P. M. S. Neves
Department of Chemistry and QOPNA, University of Aveiro
Campus de Santiago, 3810-193 Aveiro (Portugal)
E-mail: gneves@ua.pt

[b] Dr. N. M. M. Moura, Dr. C. Núñez, Prof. J. L. Capelo, Prof. C. Lodeiro
BIOSCOPE Group, REQUIMTE, Chemistry Department
Faculty of Science and Technology, University NOVA of Lisbon
2829-516, Monte da Caparica (Portugal)
E-mail: cle@fct.unl.pt

[c] Dr. N. M. M. Moura, Dr. C. Núñez, Prof. J. L. Capelo, Prof. C. Lodeiro
ProteoMass Scientific Society, Madan Parque, Rua dos Inventores
2825-182, Caparica (Portugal)

[d] Dr. C. Núñez
Department of Geographical and Life Sciences
Canterbury Christ Church University, CT1 1QU Canterbury (UK)

[e] Dr. S. M. Santos, Dr. F. A. Almeida Paz
Department of Chemistry and CICECO
University of Aveiro, Campus de Santiago, 3810-193 Aveiro (Portugal)

Supporting information for this article is available on the WWW under http://dx.doi.org/10.1002/chem.201402270.

porphyrin-2-ylmethyl moieties (**2**) from 2-formyl-5,10,15,20-tetraphenylporphyrin (**1**). Based on the ability of porphyrins to be used as fluorescent and colorimetric chemosensors and also on our research interest on this topic[20–25] we envisaged that the presence of the two porphyrinic units linked by the pyridine could potentiate the ability of the new system to recognize and to bind different metal ions.

The sensing ability of the new derivative towards Zn^{2+}, Cu^{2+}, Hg^{2+}, Cd^{2+}, and Ag^{+} was carried out in solution, gas phase, and by using solid-supported polymers. The preferential stoichiometry and binding mode in solution was confirmed by molecular dynamics simulations. In addition, the structure of Zn^{II} complex of 3,5-bis(5,10,15,20-tetraphenylporphyrin-2-ylmethyl)pyridine was unequivocally elucidated by single-crystal X-ray diffraction.

Results and Discussion

During our studies on the structural modification of *meso*-tetraarylporphyrins through a β-formyl group, we found that the simple reflux of 2-formyl-5,10,15,20-tetraphenylporphyrin **1** in toluene in the presence of piperidine affords the new 3,5-bisporphyrinylpyridine **2** in 36% yield (Scheme 1, a). A literature

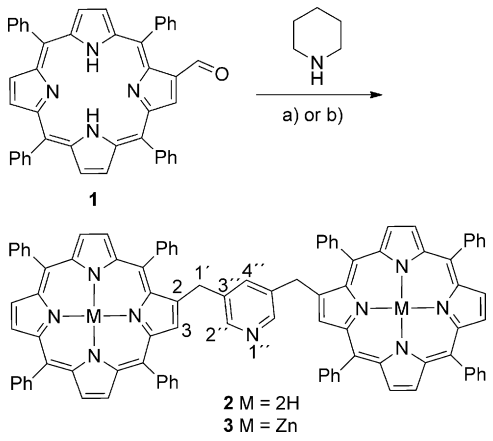

Scheme 1. Synthetic route of 3,5-bisporphyrinylpyridine **2**. Reagents and conditions: a) toluene, heat at reflux, 19 h, 36%; b) [La(OTf)$_3$], toluene, heat at reflux, 19 h, 54%.

survey showed that a similar reactivity was reported by Poirier and Burrows for simpler aldehydes like benzaldehyde and analogues.[26–28] Based on the proposed mechanism (Scheme S1 in the Supporting Information) namely electrophilic additions to the formyl group and the formation of enamines involving piperidine, and knowing the potentialities of [La(OTf)$_3$] as a Lewis acid even when water is present[29] we decided to repeat the condensation in the presence of this reagent. Under the new experimental conditions (Scheme 1, b) the desired compound **2** was isolated, after workup and purification, in a comfortable yield of 54%. The structure was unambiguously established by spectroscopic data, namely NMR spectroscopy, UV/Vis spectroscopy, and mass spectrometry techniques (see NMR spectroscopic data in the Supporting Information).

The ^{1}H NMR spectrum of this highly symmetric compound shows, in the low field region, a singlet at $\delta = 8.26$ ppm due to the H-3 proton, one AB system at $\delta = 8.83$ ppm and four doublets at $\delta = 8.74$, 8.66, 8.52, and 8.38 ppm, which correspond to the remaining β-pyrrolic protons. The signals from the pyridine moiety appear as two singlets at $\delta = 7.89$ ppm (H-2″ and H-6″) and $\delta = 6.58$ ppm (H-4″) separated from the resonances due the *meso*-phenyl protons. In the aliphatic region the singlet at $\delta = 4.10$ ppm was attributed to the resonances of the $-CH_2$ protons; the resonance of the corresponding aliphatic carbon appears in the ^{13}C NMR spectrum as distinctive signal at $\delta =$ 33.5 ppm. The proton and carbon assignments were performed with the support of 2D NMR spectroscopic techniques, namely COSY, HSQC, and HMBC (Figures S1–S5 in the Supporting Information). The MALDI mass spectrum with a peak at *m/z* 1332.4 corresponding to the molecular ion $[M+H]^+$ is also compatible with the structure of **2**. With this study it was demonstrated that lanthanum(III) triflate plays an important role in the synthesis of **2** contributing for a clean reaction and high yield of the desired compound.

The photophysical characterization of compound **2** was performed in chloroform solution at 298 K and the main photophysical data are reported in Table 1. The absorption, excitation, and emission spectra of compound **2** as well as the emission spectra obtained from the solid state of the same derivative are shown in Figure 1.

The absorption spectrum shows the typical features of free base porphyrins due to π–π* transitions with the highly in-

Table 1. Photophysical data of compound **2** in $CHCl_3$ and in solid state at 298 K.

λ_{max} [nm] (log ε [dm^3 M^{-1} cm^{-1}])	λ_{em} [nm]	Stokes shift [cm^{-1}]	Φ_{Flu}	$\lambda_{em\ solid}$ [nm]
418 (5.56) 516 (4.49) 550 (4.01) 592 (3.96) 647 (3.70)	651, 719	2.5×10^6	0.03	662, 720, 822

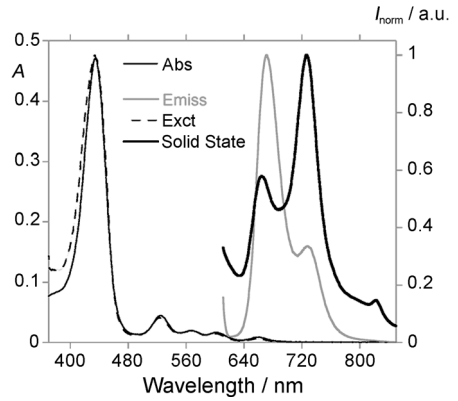

Figure 1. Absorption (Abs) and normalized emission (Emiss) and excitation (Exct) spectra of compound **2** in $CHCl_3$ ($[\mathbf{2}] = 1.00\times10^{-6}$ M, $\lambda_{exc} = 592$ nm and $\lambda_{emiss} = 719$ nm) and emission spectrum in the solid state at 298 K.

tense Soret band or B band (due to the allowed transition from $S_0 \rightarrow S_2$) at 418 nm and four weak Q bands (due to the transition from $S_0 \rightarrow S_1$) between 516 and 647 nm. The perfect match between the absorption and the excitation spectra rules out the presence of any emissive impurity. The fluorescence emission spectrum of compound **2** obtained after excitation at 592 nm presents two bands centered at 651 and 719 nm, which are characteristic of porphyrin derivatives.

Compound **2** shows a Stokes shift of 2.5×10^6 cm^{-1}, which is indicative of a change in the electronic nature of the excited state compared with that of the ground state. The fluorescence quantum yield (Φ_{Flu}), determined by the internal reference method with respect to a solution of crystal violet in methanol as a standard ($[\Phi_{Flu}] = 0.54$),[30,31] is 0.03.

The emission spectrum of the solid powder of ligand **2** was also measured by using a fiber optic system connected to the Horiba JY Scientifc Fluoromax 4. The solid-state spectrum shows fluorescence bands between 662–822 nm with maximum intensities different to the ones observed in solution.

The sensorial ability of ligand **2** towards the metal cations was studied by adding aliquots of Zn^{2+}, Cu^{2+}, Hg^{2+}, Cd^{2+}, and Ag^{+} in acetonitrile to a solution of **2** in $CHCl_3$. These titrations promoted significant changes in the ground and excited states as can be seen in Figure 2 for the studies performed with Zn^{2+} and also in Figures S6 to S8 in the Supporting Information for the other metals. After titration with all the aforementioned metal ions, a red shift of the initial Soret band centered at 418 nm was observed in the absorption spectra that varied between 425 and 443 nm. In the Q-band region the final alterations were dependent on the sensing metal. For Zn^{2+} and Cu^{2+}, only two Q bands centered at about 540 and 600 nm were detected (Figure 2 A). For Hg^{2+} and Cd^{2+} the decrease of the Q band at 516 nm is accompanied by the appearance of a new band at about 663 nm; these effects are probably due to different interactions between the metal ions and the electron lone-pair of the inner N atoms of the porphyrin macrocycle.

Considering the excited state, a decrease in the two bands centered at 652 and 716 nm, due to the free base porphyrin emission Q (0–0) and Q (0–0)(0–1)[32] was observed after the addition of the explored metal ions. However, with the addition of Zn^{2+}, such a decrease is accompanied by the appearance of a new band at 608 nm (Figure 2 B). This new emission band, which increases with the addition of Zn^{2+}, can be assigned to a metal-to-ligand charge transfer and indicates the generation of a new fluorophore arising from the metal–porphyrin association.

The alterations observed in the absorption spectrum of compound **2** upon titration with Zn^{2+} resulted in a color change from yellowish-brown to green. These data, together with the appearance of the blue-shifted emission band that leads to a remarkable color change in the emission from red to intense orange (Figure 2), can be analytically explored to develop a new type of Zn^{2+} chromogenic and fluorogenic molecular device, as it can be concluded from the comparative fluorescent response for Hg^{2+}, Cd^{2+}, Cu^{2+}, and Ag^{+}. Spectrophotometric changes were not observed after the titration of molecular probe **2** with Ag^{+}.

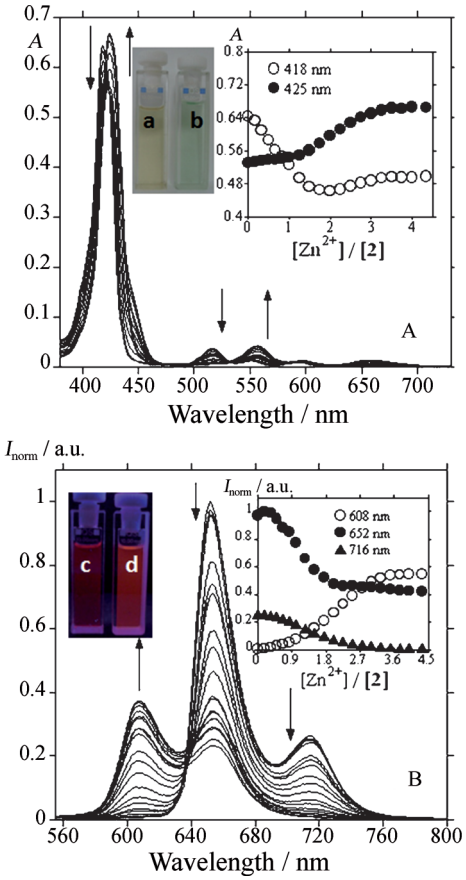

Figure 2. A) Spectrophotometric, and B) spectrofluorimetric titrations of **2** in chloroform as a function of added Zn^{2+} in acetonitrile at 298 K. The inset graphs show the absorption at 418 and 425 nm (A) and the normalized fluorescence intensity at 608, 652, and 716 nm (B) ($[\mathbf{2}] = 1.00 \times 10^{-6}$ M, $\lambda_{exc} = 536$ nm). Inset photographs a and b: solution of **2** in $CHCl_3$ before and after addition of Zn^{2+}, respectively, under visible light; c and d: solution of **2** in $CHCl_3$ before and after addition of Zn^{2+}, respectively, after excited at 365 nm by a UV lamp.

Considering the stability constants values ($\Sigma \log \beta = 15.46$–18.89) presented in Table 2 and the limit of detection (LOD; 39–99 ppb) and limit of quantification (LOQ; 79–199 ppb) values presented in Table 3, we can conclude that ligand **2** is an efficient molecular probe for the detection of Zn^{2+}, Cu^{2+}, Hg^{2+}, and Cd^{2+} metal ions; all data are in accordance with

Table 2. Stability constants for chemosensor **2** in the presence of Zn^{2+}, Cu^{2+}, Hg^{2+}, Cd^{2+}, and Ag^{+} in $CHCl_3$ for an interaction 3:1 (metal/ligand) at 298 K.

Interaction (M/L)	$\Sigma \log \beta$ (Abs)	$\Sigma \log \beta$ (Emiss)
Zn^{2+} (3:1)	$15.46 \pm 1.21 \times 10^{-3}$	$15.57 \pm 1.64 \times 10^{-2}$
Cu^{2+} (3:1)	$17.28 \pm 1.34 \times 10^{-3}$	$16.74 \pm 1.17 \times 10^{-2}$
Hg^{2+} (3:1)	$18.28 \pm 6.52 \times 10^{-3}$	$18.89 \pm 1.13 \times 10^{-2}$
Cd^{2+} (3:1)	$17.28 \pm 1.34 \times 10^{-3}$	$16.74 \pm 1.17 \times 10^{-2}$
Ag^{+}	–	–

Table 3. Limits of detection (LOD) and quantification (LOQ) in ppm for Zn^{2+}, Cu^{2+}, Hg^{2+}, Cd^{2+}, and Ag^{+} with compound **2**.

Metal ion	LOD	LOQ
Zn^{2+}	0.039 ± 0.001	0.079 ± 0.001
Cu^{2+}	0.039 ± 0.001	0.079 ± 0.001
Hg^{2+}	0.099 ± 0.001	0.199 ± 0.001
Cd^{2+}	0.068 ± 0.001	0.137 ± 0.001
Ag^{+}	–	–

a 1:3 ligand-to-metal stoichiometry (see later theoretical studies).

To confirm the high recognition efficiency of the new system, the titration of the non-substituted synthetic precursor 5,10,15,20-tetraphenylporphyrin (TPP) with Hg^{2+}, Cu^{2+}, Zn^{2+}, Cd^{2+}, and Ag^{+} (data not shown) was also performed. No significant changes were detected in the absorption and emission spectra when the same amount of the metal ion was added. To observe some changes in the ground and excited states the addition of a large amount of the metal ions (≈10 equiv) to TPP was required; the stability constants obtained for those interactions are much lower than the ones found for compound **2** (Σlog ≈ 6 vs. 17).

The sensing ability of 3,5-bisporphyrinylpyridine **2** in the gas phase, towards Zn^{2+}, Cu^{2+}, Hg^{2+}, Cd^{2+}, and Ag^{+} ions was studied by MALDI-TOF MS by using the "dried-droplet" approach and "layer-by-layer" deposition. In these studies, compound **2** was dissolved in chloroform and the metal salts in acetonitrile. The results of the MALDI-TOF MS metal ion titrations of compound **2** with the different metals are summarized in Table S1 (see the Supporting Information). In both methods the porphyrin complex acts as an internal matrix.

As an example, the MALDI-TOF MS spectra obtained after the titration of compound **2** with $AgBF_4$, is shown in Figure S9 (see the Supporting Information). Before adding the metal salt, the ion corresponding to the protonated ligand $[\mathbf{2}+H]^+$, *m/z* 1332.37 (100% relative abundance) is observed. After adding 1 equiv of Ag^+, an ion with *m/z* 1438.06 (100% relative abundance) corresponding to $[\mathbf{2}+Ag]^+$ is detected. After the addition of 2 and 3 equiv of Ag^+, the ions, $[\mathbf{2}+2Ag]^{+\cdot}$ (*m/z* 1545.11) $[\mathbf{2}+3Ag]^+$ (*m/z* 1651.72) respectively, are also formed. After the addition of 1 equiv of the respective metal ions, 1:1 metal-to-ligand species were also formed for Cu^{2+}, Zn^{2+}, and Cd^{2+} with significant relative abundances, although with lower *m/z* values (1 to 3 below the calculated values). In the same conditions for Hg^{2+} the 1:1 species were also formed but with low relative abundances. Peaks attributable to the formation of 2:1 species were obtained for all the ions, with the exception of Hg^{2+}, however 3:1 species were only detected for Cu^{2+} and Ag^+ and, in the case of the later, they were formed with low abundance. As it can be seen, this molecular probe was able to detect all metals, including Ag^+, in the gas phase.

Considering the possibility of using compound **2** as a dye in a real sensors, low-cost polymers based on polymethylmethacrylate (PMMA) were prepared in the presence and in the absence of water, according to the strategy applied for emissive lanthanide complexes.[33–37] The fluorescence emission properties of the new hybrid inorganic–organic materials were studied using an optical fiber device connected to the spectrofluorimeter.

The results obtained after spraying the film with an 1×10^{-3} M aqueous solution containing Hg^{2+} or Zn^{2+} at room temperature are shown in Figure 3. Drastic color changes were observed with both metals. In addition, it was observed quenching of the fluorescence emission of the film after spraying with a solution of Zn^{2+}, whereas an enhancement was observed in the presence of Hg^{2+}. The results obtained show a clear interaction of these metal ions with chemosensor **2**.

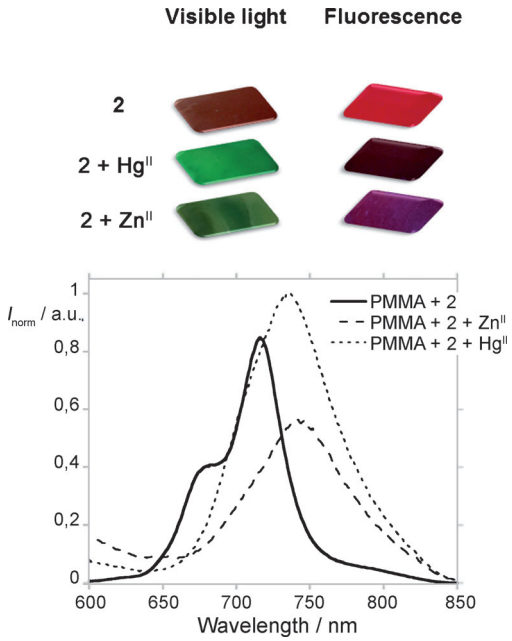

Figure 3. Visual changes observed when PMMA film with chemosensor **2** was sprayed with an aqueous solution containing Hg^{2+} or Zn^{2+} at visible light and after being excited at 365 nm using a UV lamp (top). Emission spectra of the PMMA film doped with **2** and after spraying Zn^{2+} or Hg^{2+} at room temperature (bottom).

Theoretical studies

The 3:1 binding mode of the Zn^{2+} cations to the 3,5-bisporphyrinylpyridine receptor **2**, observed in solution, was assessed, in its deprotonated form, by means of molecular dynamics simulations in explicit solvent, using classical molecular mechanics force fields. This system was chosen as being representative of the complexation modes of the receptor to the remaining metal cations. No restraints were applied to the involved species, such that the nature of the interactions between the anions (receptor and BF_4^-) and cations (Zn^{2+}) were entirely nonbonded (electrostatic and van der Waals). It should be noted that the calculation of partial atomic RESP charges for the receptor was performed using compound **3** (i.e., the receptor and two Zn^{2+} in the porphyrinic cores, as found in the single-crystal X-ray structure), for which the total charge is zero. This yielded a partial charge of +1.418 e for Zn^{2+} and

−2.835 e for the receptor: the total charges correspond to about 70% of the known formal charges of both species (+2 e and −4 e, respectively), which ultimately result in scaled-down electrostatic interactions between the cations and the receptor. All Zn^{2+} cations were, thus, assigned a partial charge of +1.418 e and those of BF_4^- (required for balancing the total charge of the system) were scaled as to yield a total charge of −0.709 e (see the Experimental Section for further details).

The lowest energy molecular-mechanics co-conformation of $\mathbf{2}^{4-}\cdot 3\,Zn^{2+}\cdot 2\,BF_4^-$ is shown in Figure 4. Two Zn^{2+} cations are located inside the porphyrinic cores, with N···Zn^{2+} distances ranging from 1.90 to 1.97 Å, whereas the third cation binds to the pyridine nitrogen, with N···Zn^{2+} distance of 1.93 Å, stabilized by the two BF_4^- counteranions. The porphyrin rings are parallel-displaced relatively to each other, such that one of the phenyl units from each porphyrin is placed above the cation inside the neighboring porphyrin, eventually stabilizing the cation through π···Zn^{2+} electrostatic interactions.

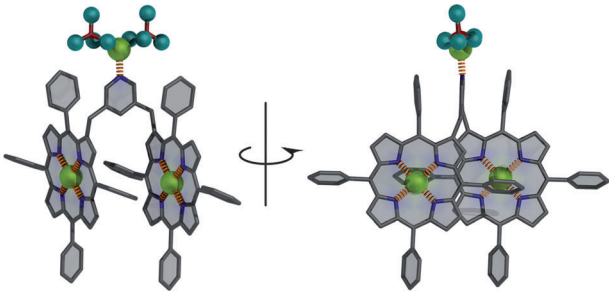

Figure 4. Lowest energy molecular mechanics co-conformation involving the three Zn^{2+} cations, the 3,5-bisporphyrinylpyridine receptor and the two BF_4^- counteranions. Hydrogen atoms have been omitted for the sake of clarity. Color code: green: Zn; blue: N; gray: C; teal: F; brown: B.

The results from five independent 20 ns long simulations, in explicit $CHCl_3$, reveal that the binding arrangement in Figure 4 is stable in solution. The spatial distribution functions of the solutes (receptor, cations, and counteranions) during the total 100 ns long simulation (all structures were fitted to a reference structure using the C and N atoms of pyridine) is shown in Figure 5. The isosurfaces encompass the totality of the positions occupied by the component atoms throughout the simulation. The Zn^{2+} cation above the pyridine shows little mobility relatively to the nitrogen atom of the pyridine, indicating that the N···Zn^{2+} interaction is conserved, whereas the isosurface corresponding to the counteranions suggest that both BF_4^- anions and the cation persist as a loosely bounded, neutral, ion-triplet. The shape of the isosurface of the counteranion indicates that the cation is relatively shielded from the solvent molecules by both counteranions, the pyridine and phenyl units of the receptor. The *meso*-phenyl units from both porphyrins neighboring the pyridine bridge seem to be almost parallel to the pyridine ring during most of the time, suggesting little mobility of this ensemble (see the Supporting Information for additional images), which can be associated with high stability of the association. It should be noted that the

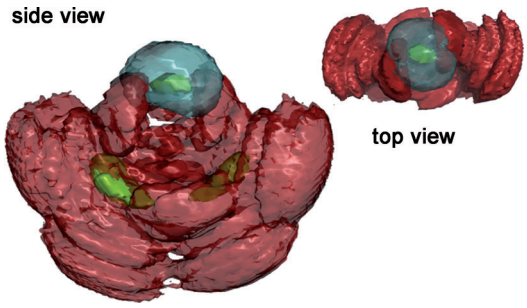

Figure 5. Spatial distribution function of the $\mathbf{2}^{4-}\cdot 3\,Zn^{2+}\cdot 2\,BF_4^-$ complex. The isosurfaces have been drawn at the 100% isolevel, meaning that they encompass the totality of the positions occupied by the involved species during the entire course of the MD simulations. Isosurfaces pertaining to the receptor, cations, and counteranions are in red, green, and teal, respectively.

scaled partial charges underestimate the electrostatic interactions between charged species, which, in this case, underestimate the highly favorable interactions between the cation and the pyridine nitrogen and the cation and the BF_4^- counteranions. It is, thus, likely that the interactions in the real case will stabilize more this association than what is being inferred from the simulation. Finally, the isosurfaces pertaining to the receptor itself and the two remaining cations indicate that both cations are kept inside the porphyrinic core, as otherwise expected. It seems that the stability of the cation-to-pyridine association can be assigned to the combined shielding effect of the two neighbor *meso*-phenyl rings and the BF_4^- counteranions, along with the polarity of the solvent. A more polar solvent such as ethanol or acetone would probably easily disrupt the whole ensemble, since the solvent molecules would easily stabilize the ionic species. This has, however, not been studied.

X-ray diffraction

The Zn^{2+} complex **3** was successfully crystallized from a mixture of CH_2Cl_2/hexane, which allowed the isolation of crystals whose structure was fully elucidated using single-crystal X-ray diffraction at 150 K (see the technical details given in the Supporting Information).[38,39] The crystal structure could be described either in the non-centrosymmetric *Cc* space group or in the centrosymmetric *C*2/*c* one. The compound contains, nevertheless, a remarkable 3,5-bisporphyrinylpyridine molecular unit composed of two 5,10,15,20-tetraphenylporphyrins bridged together by a 3,5-disubstituted pyridine as depicted in Figure 6 (see also Figure S11 in the Supporting Information for the corresponding atomic labeling). We note that the ambiguity related with the space group of this compound (see the Supporting Information for additional details) is strongly related with both the bulky nature of the 3,5-bisporphyrinylpyridine unit (which prevents an effective close packing) and the fact that the molecule is, indeed, centrosymmetric: a mirror plane bisects the bridging 3,5-disubstituted pyridine and crystallographically the two moieties could even be related by a C_2 axis (hence the *Cc* versus *C*2/*c* dichotomy for the space groups). Because the non-centrosymmetric structure describes in a much better pictorial fashion the crystal structure, the

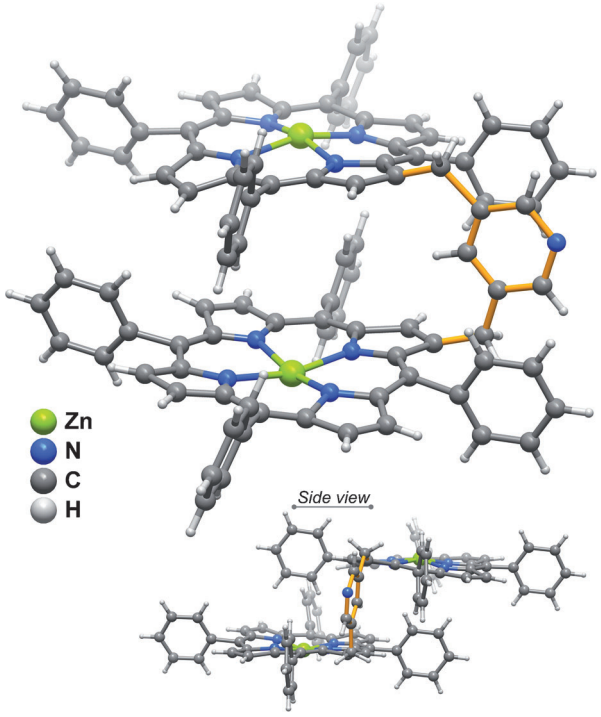

Figure 6. Perspective views of the 3,5-bisporphyrinylpyridine molecular unit composing the crystal structure of compound **3**. The interporphyrin bridge ensured by the 3,5-disubstituted pyridine is highlighted with the bonds depicted in orange. For additional drawings depicting the atomic labeling and crystal packing features see Figures S11 to S13 in the Supporting Information.

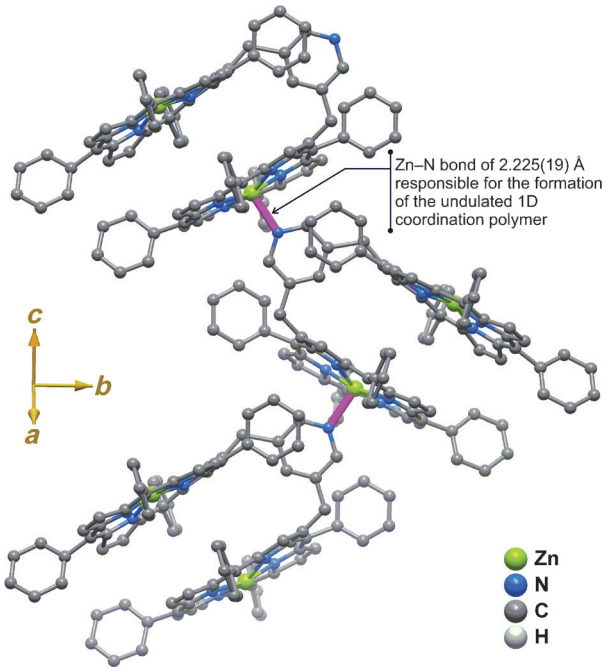

Figure 7. Fragment of the one-dimensional coordination polymer present in compound **3**, emphasizing the inter-3,5-bisporphyrinylpyridine connectivity established between the nitrogen atom of the interporphyrin bridging 3,5-disubstituted pyridine and a Zn2 cation from a neighboring 3,5-bisporphyrinylpyridine unit. The length of this connection varies slightly according to the space group in which the structure was refined, being the longest 2.225(19) Å for the centrosymmetric model (in *C*2/*c*).

structural discussion in the following paragraphs will be focused on this structural determination being, nevertheless, valid for both space groups.

In the *Cc* space group (**3_Cc**), and as expected from the chemical synthesis, the structure contains two crystallographically independent Zn^{2+} metallic centers: Zn1 is tetracoordinated to four pyrrole rings of the porphyrin molecule with an overall geometry resembling a distorted square, $\{ZnN_4\}$; Zn2 is instead five-coordinated exhibiting a typical distorted square-pyramidal coordination environment, $\{ZnN_5\}$, in which the apical position is composed of a Zn–N bond with the bridging 3,5-disubstituted pyridine of a neighboring dimer. Noteworthy, for **3_Cc** the Zn–N bonds fall within a relatively narrow range (1.943(11)–2.19(2) Å; see Figure S11 and Table S2 in the Supporting Information for detailed tabulated data), with the longer interaction corresponding to the aforementioned inter-dimer bridge (for the *C*2/*c* centrosymmetric model this bond is even slightly longer as depicted in Figure 2: 2.225(19) Å).

The inter-3,5-bisporphyrinylpyridine Zn–N coordinative bonds are at the origin of an undulated one-dimensional (1D) coordination polymer in which the 3,5-bisporphyrinylpyridine units are distributed in a zigzag herringbone fashion as shown in Figure 7 (see also Figure S12 in the Supporting Information). The coordination polymer is, in this way, highly distorted which prevents the existence of structurally significant supramolecular contacts in the crystal structure of compound **3** (Table S3, in Supporting Information, tabulates the supramolecular contacts). Consequently, the crystal packing is mostly mediated by the need to effectively fill the available space leaving, nevertheless, large voids in the structure (Figure S13 in the Supporting Information), which are filled with highly disordered solvent molecules (could not be located in the performed crystallographic studies).

The obtained results show that 3,5-bisporphyrinylpyridine **2** is a useful potential probe for metal ion detection. Species with different metal-to-ligand ratios were formed not only in the gas phase, but also in solution and in the solid state.

The main driving force for the formation of the 3:1 complex in solution may reside in entropic considerations. Although the 3:1 binding mode is favored in solution, as was found through both experiment and MD simulations, this certainly is not what happens in the solid state. In solution, the average volume occupied by the complex (receptor + cations + counteranions) is smaller than the sum of the individual component volumes, in which case the volume variation during complexation leads to a greater volume available for the solvent molecules.

Since a positive volume variation can be correlated with an increase in the entropy variation (i.e., greater ΔS), the cation-to-receptor association free energy is enhanced (i.e., made more negative) as the entropic contribution is deducted from the enthalpy ($\Delta G = \Delta H - T\Delta S$). However, as the solvent-to-solute ratio decreases, during crystallization, the greater volume variation is achieved by association of distinct receptors, mediated through the pyridine nitrogen and a core cation, eventually leading to 2:1 binding mode of the X-ray

structure. This hypothesis has not been addressed, mainly because of the methodological difficulty in calculating the entropic contributions to the association free energy.

The above considerations can explain the observed differences of stoichiometry and structure in the condensed phases. The observation of several stoichiometries in the gas phase can also be rationalized if we bear in mind that, although not observed in the present case, the ions formed when MALDI is used may include adducts with the matrix, counterions, and the solvent. In the present case no matrix was used, and the removal of several monolayers by laser ablation may lead to the formation of aggregates of neutral species, protonated and deprotonated ligands and other charged particles. The formation of the observed species is, very likely, dependent on the the different counterions and different oxidation states and ionic radii of the metal centers and probably occurs through complex aggregation/dissociation processes (involving acid/base and redox reactions) in the hot plume.

Conclusion

We have obtained and fully characterized a new 3,5-bisporphyrinylpyridine **2** through an efficient synthetic approach catalyzed by lanthanum triflate. The unexpected increase in the emission intensity of molecular probe **2** in the presence of Zn^{2+} is a very important and promising result. The ligand titration experiments with this metal cation indicate a 1:3 ligand-to-metal complex stoichiometry with a high association constant ($K_{ass} \approx 15.50$). The preferential stoichiometry and binding modes of **2** to Zn^{2+} were confirmed through theoretical calculations. Additionally, the results obtained by MALDI-TOF MS confirm the gas phase sensing abilities of **2** towards Zn^{2+}, Cu^{2+}, Hg^{2+}, Cd^{2+}, and Ag^{+}. The crystal structure of the Zn^{2+} complex **3** was fully and unequivocally elucidated by using single-crystal X-ray diffraction.

The results obtained after doping PMMA films with chemosensor **2** clearly show a promising system for the detection of Hg^{2+} and Zn^{2+} in aqueous solution, enabling **2** to discriminate between the two metal ions.

Experimental Section

General remarks

^{1}H and ^{13}C solution NMR spectra were recorded on Bruker Avance 500 (500.13 and 125.76 MHz, respectively) spectrometer. $CDCl_3$ was used as solvent and tetramethylsilane (TMS) as internal reference; the chemical shifts are expressed in δ (ppm) and the coupling constants (J) in Hertz (Hz).

Unequivocal ^{1}H assignments were made using 2D COSY ($^{1}H/^{1}H$), whereas ^{13}C assignments were made on the basis of 2D HSQC ($^{1}H/^{13}C$) and HMBC (delay for long-range J C/H couplings were optimized for 7 Hz) experiments. Mass spectra were recorded using MALDI TOF/TOF 4800 Analyzer, Applied Biosystems MDS Sciex, with $CHCl_3$ as solvent and without matrix. Mass spectra HRMS were recorded on APEXQe FT-ICR (BrukerDaltonics, Billerica, MA) mass spectrometer using $CHCl_3$ as solvent; in m/z (rel.%). Column chromatography was carried out using silica gel (Merck, 35–70 mesh). Analytical TLC was carried out on precoated sheets with silica gel (Merck 60, 0.2 mm thick).

Chemicals and starting reagents

$[Cu(BF_4)_2]\cdot 6H_2O$, $[Zn(BF_4)_2]\cdot xH_2O$, $[Cd(CF_3SO_3)_2]\cdot xH_2O$, $[Hg(CF_3SO_3)_2]\cdot xH_2O$, and $[AgBF_4]$ xH_2O were purchased from Strem Chemicals, Sigma–Aldrich, or Solchemar. All these chemicals were used without further purification. The solvents were obtained from Panreac and Riedel-de-Häen and were used as received or distilled and dried using standard procedures according to the literature procedures.[40]

Gas-phase measurements

The MALDI-MS analyses were performed in a MALDI-TOF-TOF MS model Ultraflex II (Bruker, Germany) equipped with nitrogen (BIOSCOPE group). Each spectrum represents accumulations of $5\times$ 50 laser shots. The reflection mode was used. The ion source and flight tube pressure were less than 1.80×10^{-7} and 5.60×10^{-8} Torr, respectively. The MALDI mass spectra of the soluble samples (1 or 2 $\mu g\,\mu L^{-1}$) were recorded by using the "dried droplet" and the "layer-by-layer" sample preparation methods. In both methods the ligands were dissolved in chloroform and the metal salts in acetonitrile but the introduction in the sample holder was different. In the "dried-droplet" method, the two solutions containing the ligand (1 μL) and the metal salt (1 μL) were mixed and then applied in the MALDI-TOF MS sample holder. In the "layer-by-layer" method, a solution of each ligand was spotted in the MALDI-TOF plate and then dried; subsequently, 1 μL of the solution containing the metal salt was placed on the sample holder, which was then inserted in the ion source. In this case, the chemical reaction between the ligand and the metal salts occurred in the holder, and the complex species were produced in gas phase.

Spectrophotometric and spectrofluorimetric measurements

Absorption spectra were recorded on a JASCO V-650 spectrophotometer and fluorescence emission spectra were recorded on a Horiba Jobin–Yvon Fluoromax 4 spectrofluorimeter from the BIOSCOPE group. The linearity of the fluorescence emission versus the concentration was checked in the concentration range used (10^{-4}–10^{-6} M). The correction of the absorbed light was performed when it was considered necessary. The spectrophotometric characterizations and titrations were performed by preparing a stock solution of the compound in chloroform (ca., 10^{-3} M) in a 10 mL volumetric flask. The studied solutions were prepared by appropriate dilution of the stock solution up to 10^{-5}–10^{-6} M. Titrations of molecular probe **2** were carried out by the addition of microliter amounts of standard solutions of the metal ions (Zn^{2+}, Cu^{2+}, Hg^{2+}, Cd^{2+}, and Ag^{+}) in acetonitrile. All the measurements were performed at 298 K.

Luminescence quantum yields of compound **2** were measured using a solution of crystal violet in methanol as standard ($[\Phi] = 0.54$),[30,31] and all values were corrected taking in account the solvent refractions index.

The stability constants for the interaction of ligand **2** with Zn^{2+}, Cu^{2+}, Hg^{2+}, Cd^{2+}, and Ag^{+} were calculated by using HypSpec software.[41]

Fluorescence spectra of solid samples were recorded using a fiber optic system connected to a Horiba Jobin–Yvon Fluoromax 4 spectrofluorimetric exciting the solid compound **2** at $\lambda = 592$ nm. The limit of detection (LOD) and the limit of quantification (LOQ) for metal ions were performed having in mind their use for real anion

detection and for analytical applications. For these measurements, ten different analyses for the selected receptor were performed in order to obtain the LOQ. The LOD was obtained by the formula:

$$ydl = yblank + 3\,std$$

in which ydl is the signal detection limit and std is the standard deviation.

Preparation of PMMA polymer films doped with compound 2

The preparation of the PMMA films was performed by dissolving the PMMA powder (0.1 g) in chloroform, followed by addition of compound **2** (0.001–0.005 g) dissolved in the same solvent. The polymer films were obtained after solvent evaporation at 40 °C under vacuum for 24 h.[42,43] Due to the spectroscopic characteristics the films doped with 0.005 g of the ligand **2** were selected for the studies with the metal ions.

Synthesis of the organic ligand

Synthesis of the precursor porphyrin: The 2-formyl-5,10,15,20-tetraphenylporphyrin **1** was prepared from 5,10,15,20-tetraphenylporphyrinatocopper(II), *N,N′*-dimethylformamide (DMF) and phosphorus oxychloride ($POCl_3$), according to literature procedure.[44]

Synthesis of 3,5-bis(5,10,15,20-tetraphenylporphyrin-2-ylmethyl)pyridine: [La(OTf)$_3$] (20 mol%, 4.6 μmol, 2.7 mg) and piperidine (1.5 equiv, 35.0 μmol, 3.6 μL) were added to a solution of 2-formyl-5,10,15,20-tetraphenylporphyrin (23.0 μmol, 15.0 mg) in dry toluene (2.0 mL), which was then heated at reflux for 19 h. After cooling, the reaction mixture was washed with water and extracted with chloroform. The organic phase was dried (Na_2SO_4) and the solvent was evaporated under reduced pressure. The crude mixture was submitted to column chromatography (silica gel) using toluene as eluent. The compound **2** was isolated in 54% yield and full characterized by NMR spectroscopy, mass spectrometry and UV/Vis techniques.

3,5-Bis(5,10,15,20-tetraphenylporphyrin-2-ylmethyl)pyridine (2): ^{1}H NMR (500 MHz, $CDCl_3$): $\delta = 8.83$ (4H, AB, $J = 4.8$ Hz, H-β), 8.74 (2H, d, $J = 4.8$ Hz, H-β), 8.66 (2H, d, $J = 4.8$ Hz, H-β), 8.52 (2H, d, $J = 4.8$ Hz, H-β), 8.38 (2H, d, $J = 4.8$ Hz, H-β), 8.26 (2H, s, H-3), 8.26–8.15 (8H, m, H-*o*-Ph), 7.89 (2H, s, H-2″ and H-6″), 7.76–7.61 (20H, m, H-*o,m,p*-Ph), 7.45 (2H t, $J = 7.6$ Hz, H-*m,p*-Ph), 7.35 (2H t, $J = 7.6$ Hz, H-*m,p*-Ph), 7.27 (4H, t, $J = 7.7$ Hz, H-*m,p*-Ph), 7.10 (4H, t, $J = 7.7$ Hz, Ar-H-*m, p*-Ph), 6.58 (1H, s, H-4″), 4.10 (4H, s, H-1′), −2.79 ppm (4H, s, N-H);^{13}C NMR (125 MHz, $CDCl_3$): $\delta = 147.5$ (C-2″), 142.2, 142.1, 141.8, 141.4, 135.9 (*C*-4″), 135.8, 134.6, 134.5, 134.1, 133.3, 131.9, 130.6, 129.0, 128.2, 128.0, 127.7, 127.3, 126.8, 126.65, 126.61, 126.2, 120.5, 120.1, 119.6, 119.0, 33.5 ppm (C-1′); UV/Vis ($CHCl_3$): λ_{max} ($\log\varepsilon$) = 418.0 (5.56), 516.0 (4.49), 550.0 (4.01), 592.0 (3.96), 647.0 nm (3.70 $dm^3\,м^{-1}\,cm^{-1}$); MS (MALDI): 1332.4 $[M+H]^+$; HRMS-ESI: *m/z* calcd (%) for $C_{95}H_{66}N_9$: 1332.5441 $[M+H]^+$; found: 1332.5395.

Theoretical studies

Atomic parameters for the 3,5-bisporphyrinylpyridine receptor and the zinc cation were taken from the GAFF force field[45] using Antechamber,[46] whereas chloroform was described with parameters taken from Fox et al.[47] Parameters for the BF_4^- anions were those described by Wenchuan Wang and co-workers.[48] Calculation of atomic RESP[49] fitted partial charges for the receptor were calculated on compound **3** (i.e., the receptor and two Zn^{2+} in the porphyrinic cores, for which the total charge is zero), at the HF/6–31G*//B3LYP/6–31G* level using Gaussian 09, revision A.02.[50] This procedure yielded a partial charge of +1.418 e for Zn^{2+} and −2.835 e for the receptor. To obtain a neutral system, the partial charges of BF_4^- were scaled as to yield a total charge of −0.709 e ($2q_{BF4} + q_{rec} + 3q_{Zn} = 0.0$ e). Simulation boxes (ca., $64.5\times64.5\times64.5$ Å^3 after equilibration) were constructed from one receptor, three cations and two counteranions inside a cubic box containing 2058 chloroform molecules. Simulations began with an initial solvent minimization procedure for the removal of close contacts between solute and solvent molecules, with the solute placed under strong positional restraints. The restraints were then removed, and the whole system was allowed to relax. Subsequently, a weak positional restraint was applied to the solute, and the system was heated to 300 K in the NVT ensemble for 0.5 ns, using the "velocity rescaling with stochastic term" thermostat ($\tau_{coupling} = 2.0$ ps), and equilibrated under the NPT ensemble during 2 ns using the Berendsen barostat ($\tau_{coupling} = 5.0$ ps) until the density of the system was brought to a plateau. The positional restraints used throughout both heating and equilibration procedures were definitely removed during the data collection period (5 independent 20 ns in the NPT ensemble). The LINCS algorithm was used to constrain all hydrogen involving bond distances at their equilibrium values; periodic boundary conditions, along with a 10 Å nonbonded cutoff were used; long-range electrostatic interactions were calculated with the particle mesh Ewald (PME) method; snapshots were collected every 0.2 ps. Prior to the calculation of the spatial distribution functions, all trajectories were concatenated and fitted to the first structure in the trajectory using the pyridine heavy atoms (C,N). The isosurfaces were drawn at the 100% isolevel, meaning that they encompass the totality of the positions occupied by the solute atoms during the course of the simulations.

Crystallization of the Zn^{2+} derivative of 3,5-bis(5,10,15,20-tetraphenylporphyrin-2-ylmethyl)pyridine 3

Compound **2** was dissolved in a minimal amount of CH_2Cl_2 in a vial. A few drops of $[Zn(BF_4)_2]\cdot x H_2O$ in CH_3CN were added to this solution and a change in the mixture color from brown to green was observed in accordance with the formation of complex **3**. The vial was filled with hexane and sealed. From the crystallization process was obtained the crystal of the Zn^{2+} derivative of 3,5-bis(5,10,15,20-tetraphenylporphyrin-2-ylmethyl)pyridine (**3**), which was fully elucidated by using single-crystal X-ray diffraction.

Acknowledgements

Authors are grateful to the Universidade de Aveiro, Fundação para a Ciência e a Tecnologia (FCT), European Union, QREN, FEDER and COMPETE for funding the QOPNA research unit (project PEst-C/QUI/UI0062/2013, FCOMP-01-0124-FEDER-037296). We acknowledge the Portuguese National NMR Network (RNRMN), supported by funds from FCT, Scientific PROTEOMASS Association (Portugal), CICECO (PEst-C/CTM/LA0011/2013, FCOMP-01-0124-FEDER-037271) and REQUIMTE (PEst-C/EQB/La0006/2013) for general funding and Fundação para a Ciência e a Tecnologia (FCT) for specific funding towards the purchase of the single-crystal X-ray diffractometer. N.M.M.M. and S.M.S. thank FCT/MEC for their Postdoctoral grant SFRH/BPD/84216/2012 and SFRH/BPD/64752/2009. C.N. thanks the Xunta de Galicia (Spain) for her postdoctoral contract (I2C pro-

gram). We thank M. Graça O. Santana-Marques for the helpful comments and discussion on MALDI-TOF MS studies.

Keywords: fluorescent probes · porphyrinoids · sensors · X-ray diffraction · zinc

[1] K. M. Kadish, K. M. Smith, R. Guilard, in *Handbook of Porphyrin Science, Vols. 10–12*, World Scientific Publishing Company, Singapore, **2010**.
[2] Y.-Q. Weng, F. Yue, Y.-R. Zhong, B.-H. Ye, *Inorg. Chem.* **2007**, *46*, 7749–7755.
[3] C.-Y. Li, X.-B. Zhang, Y.-Y. Dong, Q.-J. Ma, Z.-X. Han, Y. Zhao, G.-L. Shen, R.-Q. Yu, *Anal. Chim. Acta* **2008**, *616*, 214–221.
[4] N. Kaur, S. Kumar, *Tetrahedron* **2011**, *67*, 9233–9264.
[5] J. S. Kim, D. T. Quang, *Chem. Rev.* **2007**, *107*, 3780–3799.
[6] L.-J. Fan, Y. Zhang, C. B. Murphy, S. E. Angell, M. F. L. Parker, B. R. Flynn, W. E. Jones, Jr., *Coord. Chem. Rev.* **2009**, *253*, 410–422.
[7] L. N. Neupane, J.-Y. Park, J. H. Park, K.-H. Lee, *Org. Lett.* **2013**, *15*, 254–257.
[8] P. Roy, K. Dhara, M. Manassero, J. Ratha, P. Banerjee, *Inorg. Chem.* **2007**, *46*, 6405–6412.
[9] G. Crivat, K. Kikuchi, T. Nagano, T. Priel, M. Hershfinkel, I. Sekler, N. Rosenzweig, Z. Rosenzweig, *Anal. Chem.* **2006**, *78*, 5799–5804.
[10] A. Xu, K.-H. Baek, H. N. Kim, J. Cui, X. Qian, D. R. Spring, I. Shin, J. Yoon, *J. Am. Chem. Soc.* **2010**, *132*, 601–610.
[11] Z. Xu, J. Yoon, R. Spring, *Chem. Soc. Rev.* **2010**, *39*, 1996–2006.
[12] Y. Yang, J. Jiang, G. Shen, R. Yu, *Anal. Chim. Acta* **2009**, *636*, 83–88.
[13] D. W. Boening, *Chemosphere* **2000**, *40*, 1335–1351.
[14] M. V. B. Krishna, M. Ranjit, D. Karunasagar, J. Arunachalam, *Talanta* **2005**, *67*, 70–80.
[15] T. W. Clarkson, L. Magos, G. J. Myers, *N. Engl. J. Med.* **2003**, *349*, 1731–1737.
[16] P. Grandjean, P. Weihe, R. F. White, F. Debes, *Environ. Res.* **1998**, *77*, 165–172.
[17] a) H. N. Kim, W. X. Ren, J. S. Kim, J. Yoon, *Chem. Soc. Rev.* **2012**, *41*, 3210–3244; b) H.-Y. Luo, X.-B. Zhang, J.-H. Jiang, C.-Y. Li, J. Peng, G.-L. Shen, R.-Q. Yu, *Anal. Sci.* **2007**, *23*, 551–555.
[18] N. M. M. Moura, C. Nuñez, S. M. Santos, M. A. F. Faustino, J. A. S. Cavaleiro, M. G. P. M. S. Neves, J. L. Capelo, C. Lodeiro, *ChemPlusChem* **2013**, *78*, 1230–1243.
[19] J. A. S. Cavaleiro, A. C. Tomé, M. G. P. M. S. Neves, in *Handbook of Porphyrin Science, Vol. 2* (Eds.: K. M. Kadish, K. M. Smith, R. Guilard), World Scientific Publishing Company, Singapore, **2010**, pp. 193–294.
[20] C. Lodeiro, F. Pina, *Coord. Chem. Rev.* **2009**, *253*, 1353–1383.
[21] C. Lodeiro, J. L. Capelo, J. C. Mejuto, E. Oliveira, H. M. Santos, B. Pedras, C. Nuñez, *Chem. Soc. Rev.* **2010**, *39*, 2948–2976.
[22] C. Nuñez, R. Bastida, A. Macías, L. Valencia, J. Ribas, J. L. Capelo, C. Lodeiro, *Dalton Trans.* **2010**, *39*, 7673–7683.
[23] C. I. M. Santos, E. Oliveira, J. F. B. Barata, M. A. F. Faustino, J. A. S. Cavaleiro, M. G. P. M. S. Neves, C. Lodeiro, *J. Mater. Chem.* **2012**, *22*, 13811–13819.
[24] C. I. M. Santos, E. Oliveira, J. C. J. M. D. S. Menezes, J. F. B. Barata, M. A. F. Faustino, V. F. Ferreira, J. A. S. Cavaleiro, M. G. P. M. S. Neves, C. Lodeiro, *Tetrahedron* **2014**, *70*, 3361–3370.
[25] C. Núñez, M. Diniz, A. A. Dos Santos, J. L. Capelo, C. Lodeiro, *Dyes Pigm.* **2014**, *101*, 156–163.
[26] R. H. Poirier, R. D. Morin, M. McKim, E. Bearse, *J. Org. Chem.* **1961**, *26*, 4275–4278.
[27] E. P. Burrows, R. F. Hutton, W. D. Burrows, *J. Org. Chem.* **1962**, *27*, 316–317.
[28] W. D. Burrows, E. P. Burrows, *J. Org. Chem.* **1963**, *28*, 1180–1182.
[29] C. Alonso, V. I. V. Serra, M. G. P. M. S. Neves, A. C. Tomé, A. M. S. Silva, F. A. A. Paz, J. A. S. Cavaleiro, *Org. Lett.* **2007**, *9*, 2305–2308.
[30] I. B. Berlman, in *Handbook of Fluorescence Spectra of Aromatic Molecules*, 2nd ed., Academic Press, New York, **1971**.
[31] M. Montalti, A. Credi, L. Prodi, M. T. Gandolfi, in *Handbook of Photochemistry*, 3rd ed., Taylor & Francis, Boca Raton, **2006**.
[32] Z.-X. Han, H.-Y. Luo, X.-B. Zhang, R.-M. Kong, G.-L. Shen, R.-Q. Yu, *Spectrochim. Acta Part A* **2009**, *72*, 1084–1088.
[33] M. D. McGehee, T. Bergstedt, C. Zhang, A. P. Saab, M. B. O'Regan, G. C. Bazan, V. I. Srdanov, A. J. Heeger, *Adv. Mater.* **1999**, *11*, 1349–1354.
[34] J. Kai, D. F. Parrab, H. F. Brito, *J. Mater. Chem.* **2008**, *18*, 4549–4554.
[35] A. Balamurugan, M. L. P. Reddy, M. Jayakannan, *J. Phys. Chem. B* **2009**, *113*, 14128–14138.
[36] J. C. Boyer, N. J. J. Johnson, F. C. J. M. van Veggel, *Chem. Mater.* **2009**, *21*, 2010–2012.
[37] H. Zhang, H. Song, B. Dong, L. Han, G. Pan, X. Bai, L. Fan, S. Lu, H. Zhao, F. Wang, *J. Phys. Chem. C* **2008**, *112*, 9155–9162.
[38] See also the Supporting Information: experimental details on the single-crystal X-ray diffraction studies performed for compound **3** (structural description in the non-centrosymmetric *Cc* and the centrosymmetric *C2/c* space groups); additional structural drawings of the crystal structure of the non-centrosymmetric model for **3** emphasizing the arrangement of individual units to form the one-dimensional polymer; tabulated geometrical data for the two crystallographically independent Zn^{2+} centers and supramolecular contacts present in the non-centrosymmetric model.
[39] Crystal data for **3_Cc** (SQUEEZE data): $C_{95}H_{61}N_9Zn_2$, $M_r = 1459.27$, monoclinic, space group *Cc*, $Z = 4$, $a = 29.978(4)$, $b = 18.696(3)$, $c = 18.525(3)$ Å, $\beta = 117.550(6)^\circ$, $V = 9205(2)$ Å^3, $\mu(Mo_{K\alpha}) = 0.566$ mm^{-1}, $\rho_{calcd} = 1.053$ g cm^{-3}. Collected reflections 30936; independent reflections 14387 ($R_{int} = 0.1127$). Crystal size $0.18 \times 0.10 \times 0.05$ mm^3. Final $R1 = 0.0973$ [$I > 2\sigma(I)$] and $wR2 = 0.2143$ (all data). Data completeness to $\theta = 25.35^\circ$, 98.8%. Crystal data for **3_C2/c** (SQUEEZE data): $C_{95}H_{61}N_9Zn_2$, $M_r = 1459.27$, monoclinic, space group *C2/c*, $Z = 4$. Collected reflections 30935; independent reflections 8337 ($R_{int} = 0.1313$). Final $R1 = 0.0997$ [$I > 2\sigma(I)$] and $wR2 = 0.2545$ (all data). Data completeness to $\theta = 25.35^\circ$, 98.8%. CCDC-941872 (**3_Cc**) and CCDC-941873 (**3_C2/c**) contain the supplementary crystallographic data for this paper. These data can be obtained free of charge from The Cambridge Crystallographic Data Centre via www.ccdc.cam.ac.uk/data_request/cif.
[40] W. L. F. Armarego, D. D. Perrin, in *Purification of Laboratory Chemicals*, 4th ed., Butterworth-Heinemann, Oxford, **1996**.
[41] P. Gans, A. Sabatini, A. Vacca, *Talanta* **1996**, *43*, 1739–1753.
[42] D. B. A. Raj, B. Francis, M. L. P. Reddy, R. R. Butorac, V. M. Lynch, A. H. Cowley, *Inorg. Chem.* **2010**, *49*, 9055–9063.
[43] O. Moudam, B. C. Rowan, M. Alamiry, P. Richardson, B. S. Richards, A. C. Jones, N. Robertson, *Chem. Commun.* **2009**, 6649–6651.
[44] N. M. M. Moura, M. A. F. Faustino, M. G. P. M. S. Neves, A. C. Duarte, J. A. S. Cavaleiro, *J. Porphyrins Phthalocyanines* **2012**, *16*, 652–658.
[45] J. M. Wang, R. M. Wolf, J. W. Caldwell, P. A. Kollman, D. A. Case, *J. Comput. Chem.* **2004**, *25*, 1157–1174.
[46] J. M. Wang, W. Wang, P. A. Kollman, D. A. Case, *J. Mol. Graphics Modell.* **2006**, *25*, 247–260.
[47] T. Fox, P. A. Kollman, *J. Phys. Chem. B* **1998**, *102*, 8070–8079.
[48] a) C. I. Bayly, P. Cieplak, W. D. Cornell, P. A. Kollman, *J. Phys. Chem.* **1993**, *97*, 10269–10280; b) W. D. Cornell, P. Cieplak, C. I. Bayly, P. A. Kollman, *J. Am. Chem. Soc.* **1993**, *115*, 9620–9631.
[49] X. Wu, Z. Liu, S. Huang, W. Wang, *Phys. Chem. Chem. Phys.* **2005**, *7*, 2771–2779.
[50] Gaussian 09, Revision A.02, M. J. Frisch, G. W. Trucks, H. B. Schlegel, G. E. Scuseria, M. A. Robb, J. R. Cheeseman, G. Scalmani, V. Barone, B. Mennucci, G. A. Petersson, H. Nakatsuji, M. Caricato, X. Li, H. P. Hratchian, A. F. Izmaylov, J. Bloino, G. Zheng, J. L. Sonnenberg, M. Hada, M. Ehara, K. Toyota, R. Fukuda, J. Hasegawa, M. Ishida, T. Nakajima, Y. Honda, O. Kitao, H. Nakai, T. Vreven, J. A. Montgomery, Jr., J. E. Peralta, F. Ogliaro, M. Bearpark, J. J. Heyd, E. Brothers, K. N. Kudin, V. N. Staroverov, R. Kobayashi, J. Normand, K. Raghavachari, A. Rendell, J. C. Burant, S. S. Iyengar, J. Tomasi, M. Cossi, N. Rega, J. M. Millam, M. Klene, J. E. Knox, J. B. Cross, V. Bakken, C. Adamo, J. Jaramillo, R. Gomperts, R. E. Stratmann, O. Yazyev, A. J. Austin, R. Cammi, C. Pomelli, J. W. Ochterski, R. L. Martin, K. Morokuma, V. G. Zakrzewski, G. A. Voth, P. Salvador, J. J. Dannenberg, S. Dapprich, A. D. Daniels, O. Farkas, J. B. Foresman, J. V. Ortiz, J. Cioslowski, D. J. Fox, Gaussian Inc., Wallingford CT, 2009.

Received: February 20, 2014
Published online on April 29, 2014

